Evidence of power-law flow in the Mojave desert mantle

Andrew M. Freed[1] **& Roland Bürgmann**[2]

[1]*Department of Earth and Atmospheric Sciences, Purdue University, West Lafayette, Indiana 47907, USA*
[2]*Department of Earth and Planetary Science, University of California, Berkeley, Berkeley, California 94720, USA*

Studies of the Earth's response to large earthquakes can be viewed as large rock deformation experiments in which sudden stress changes induce viscous flow in the lower crust and upper mantle that lead to observable postseismic surface deformation[1]. Laboratory experiments suggest that viscous flow of deforming hot lithospheric rocks is characterized by a power law in which strain rate is proportional to stress raised to a power, n (refs 2, 3). Most geodynamic models of flow in the lower crust and upper mantle, however, resort to newtonian (linear) stress–strain rate relations[4–10]. Here we show that a power-law model of viscous flow in the mantle with $n = 3.5$ successfully explains the spatial and temporal evolution of transient surface deformation following the 1992 Landers[11] and 1999 Hector Mine[12] earthquakes in southern California. A power-law rheology implies that viscosity varies spatially with stress causing localization of strain, and varies temporally as stress evolves, rendering newtonian models untenable. Our findings are consistent with laboratory-derived flow law parameters for hot and wet olivine—the most abundant mineral in the upper mantle—and support the contention that, at least beneath the Mojave desert[5,6], the upper mantle is weaker than the lower crust.

High-temperature, high-pressure creep experiments suggest that warm rocks deform by a thermally activated flow law of the form:

$$\dot{\varepsilon} = A\sigma^n e^{(-Q/RT)} \quad (1)$$

where $\dot{\varepsilon}$ is strain rate (s^{-1}), A is a pre-exponential factor ($MPa^{-n}s^{-1}$), σ is the differential stress (MPa), n is the power-law exponent, Q is the activation energy ($kJ\,mol^{-1}$), R is the universal gas constant ($J\,mol^{-1}K^{-1}$), and T is temperature (K)[2,3]. Laboratory experiments suggest that for conditions associated with the lower crust and the upper ~200 km of the mantle[13], flow should be accommodated by dislocation creep (involving dislocation glide and recovery processes such as dislocation climb), where the exponent, n, is usually between 2 and 4 (refs 2, 3). Dislocation creep is supported by preferred mineral-axis orientations inferred from observations of seismic anisotropy[14] and similarities between microstructures observed in naturally and experimentally deformed rocks[15].

The effective viscosity ($\eta = \sigma/2\dot{\varepsilon}$) of a power-law material is given by:

$$\eta = \sigma^{(1-n)} e^{(Q/RT)}/2A \quad (2)$$

The stress dependence in equation (2) implies that viscosities decrease when stresses increase, such as immediately below and after an earthquake. Pre-earthquake viscosities will be restored as earthquake-related stresses are dissipated by viscous flow. With a high power-law exponent ($n > 3$), the coseismic decrease in viscosity can be quite significant, inducing very rapid early postseismic strain rates. Compared to newtonian ($n = 1$) rheologies, the reduction of postseismic strain rates associated with power-law flow would be highly accelerated. Thus, a close monitoring of deformation rates as a function of time, such as that provided by global positioning system (GPS) time-series data, can serve as a diagnostic test to differentiate between power-law and newtonian rheologies.

A hint as to the nonlinear nature of postseismic flow was evident in previous newtonian studies of the 1992 $M_w = 7.3$ Landers and 1999 $M_w = 7.1$ Hector Mine earthquakes that occurred in the Mojave desert of southern California. In a post-Hector Mine study[5], the inferred average viscosity for the first eight months of postseismic relaxation was an order of magnitude smaller than that inferred from deformation measurements spanning a three-year period starting three months after the Landers earthquake[6], leading Pollitz *et al.*[5] to infer a nonlinear rheology. Refs 16 and 7 also suggested the possibility of nonlinear rheology on the basis of observations of strain-rate change in post-Hector Mine and post-1906 San Francisco earthquake time-series data, respectively.

The Landers and Hector Mine earthquakes occurred only 20 km apart, making it likely that the postseismic observations of both events result from the response of the same lithosphere. The coupled nature of these earthquakes thus makes them ideal for a stringent rheology study in that a candidate rheologic model must satisfy the postseismic observations associated with both events. We focus here on two particular data sets that allow us to address the evolution of deformation with time: nine repeatedly surveyed campaign GPS

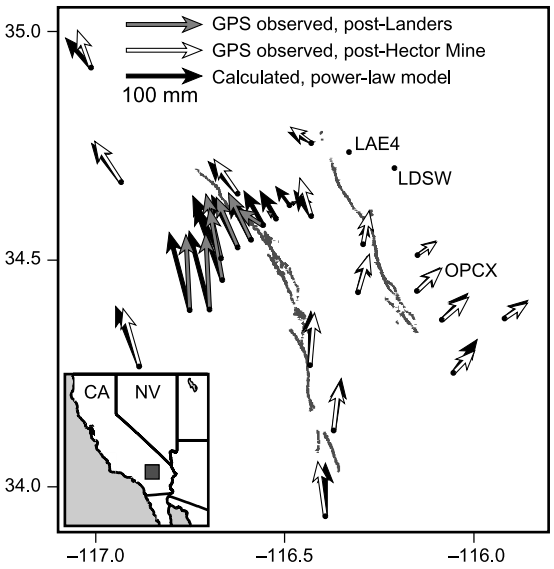

Figure 1 GPS observed and calculated horizontal postseismic surface displacements following the 1992 Landers and 1999 Hector Mine earthquakes in the Mojave desert of southern California. Two separate GPS data sets are used: campaign data following the Landers earthquake[11] and continuous data following the Hector Mine earthquake[12]. The campaign data (grey arrows) are shown relative to station LAE4, while the continuous data (white arrows) are relative to station LDSW. Post-Landers campaign data (Emerson transect) span July 1992 through to February 1998. Post-Hector Mine continuous data span October 1999 through to December 2002. Calculated displacements are based on a finite element model that incorporates a power-law rheology of predominately mantle flow (model 8 in Fig. 2, see Table 1 for power-law parameters).

Table 1 **Laboratory-derived power-law parameters considered in this analysis**

Rock type	A ($MPa^{-n}s^{-1}$)	N	Q ($kJ\,mol^{-1}$)	Reference number
Wet quartzite1	2.2×10^{-6}	2.7	120	25
Wet quartzite2	6.3×10^{-12}	4.0	135	15
Dry quartzite 1	1.0×10^{-3}	2.0	167	26
Dry quartzite 2	3.1×10^{-4}	2.3	171	27
Aplite	3.3×10^{-7}	3.1	163	26
Quartz-diorite	1.3×10^{-3}	2.4	219	28
Anorthosite	3.2×10^{-4}	3.2	238	26
Diabase	2.2×10^{-4}	3.4	260	26
Dry olivine	1.1×10^{4}	3.5	535	29
Wet olivine*	3.6×10^{5}	3.5	480	29

*For wet olivine, we fold water content into the A term by using the formulation $A^* = AC_{OH}^b$, where we assume constant $C_{OH} = 1{,}000H/106Si$ and use $A = 90\,MPa^{-3.5}s^{-1}$ and $b = 1.2$ from ref. 29.

stations along the USGS Emerson transect[11] provide time series spanning both earthquakes, and 18 continuous SCIGN GPS stations provide highly precise and temporally dense measurements following the Hector Mine earthquake[12] (Fig. 1).

To infer the nature of viscous flow beneath the Mojave desert we developed a finite element model of the Landers and Hector Mine sequence that simulates coseismic slip associated with both events[17,18], a regional background strain rate, and rheologic models that consider both newtonian and temperature-dependent power-law rheologies. Our approach builds on our previous newtonian modelling studies of rheology and earthquake stress transfer associated with the Landers and Hector Mine sequence[8,9].

Previous analyses have suggested near-field (within 10–20 km) post-Landers deformation could be explained by a combination of poroelastic rebound and lower crustal flow[19] or a combination of poroelastic rebound and afterslip[20]. However, our modelling suggests that using poroelastic rebound in conjunction with viscous flow or afterslip to explain near-field post-Landers surface deformations leads to a significant underprediction of post-Landers far-field deformations (see Supplementary Fig. 1) and a pattern of post-Hector Mine surface deformations inconsistent with observations (see Supplementary Fig. 2a). In addition, the stability of the azimuth of post-Hector Mine GPS motions (see Supplementary Fig. 2b) and InSAR deformation patterns[5] support a single dominant deformation mechanism. We therefore consider a simpler (only one mechanism) yet advanced model that assumes power-law flow. Nevertheless, the potential contributions of multiple mechanisms cannot be ruled out.

Our analysis seeks to determine the combination of thermal gradient and assumed power laws that are consistent with the observed heat flow, geology and seismic velocities in the region, as well as with the observed postseismic deformation. We consider a range of power laws (Table 1) reflecting uncertainty in the mineralogy of the lithosphere and extrapolation from laboratory to geological conditions. Thermal gradients for the Mojave crust are estimated by assuming conductive heat transfer constrained by surface heat flow measurements that range from 52 to 69 mW m^{-2}, leading to inferred temperatures of 520 ± 50 to 780 ± 50 °C at the base of a 30-km-thick crust[21]. Below the crust we assume a rapid transition to an adiabatic temperature gradient (0.5 °C km^{-1}) in the shallow upper mantle based on seismic velocities that suggest a thin (5 to 10-km-thick) mantle lid overlying relatively shallow, and probably convecting, asthenosphere[6,22]. These constraints lead us to consider a range of possible thermal gradients for the Mojave region, as shown in Fig. 2a.

Because power-law viscosity is dependent upon the absolute stress field, we begin each calculation by applying an inferred regional strain rate until steady-state stress levels are achieved in

Model number	Crust	Mantle
1	wet quartzite 1	dry olivine
2	dry quartzite 1	dry olivine
3	dry quartzite 2	dry olivine
4	wet quartzite 1	wet olivine
5	dry quartzite 1	wet olivine
6	dry quartzite 2	wet olivine
7	quartz-diorite	wet olivine
8	aplite	wet olivine
9	wet quartzite 2	wet olivine
10	anorthosite	wet olivine
11	diabase	wet olivine

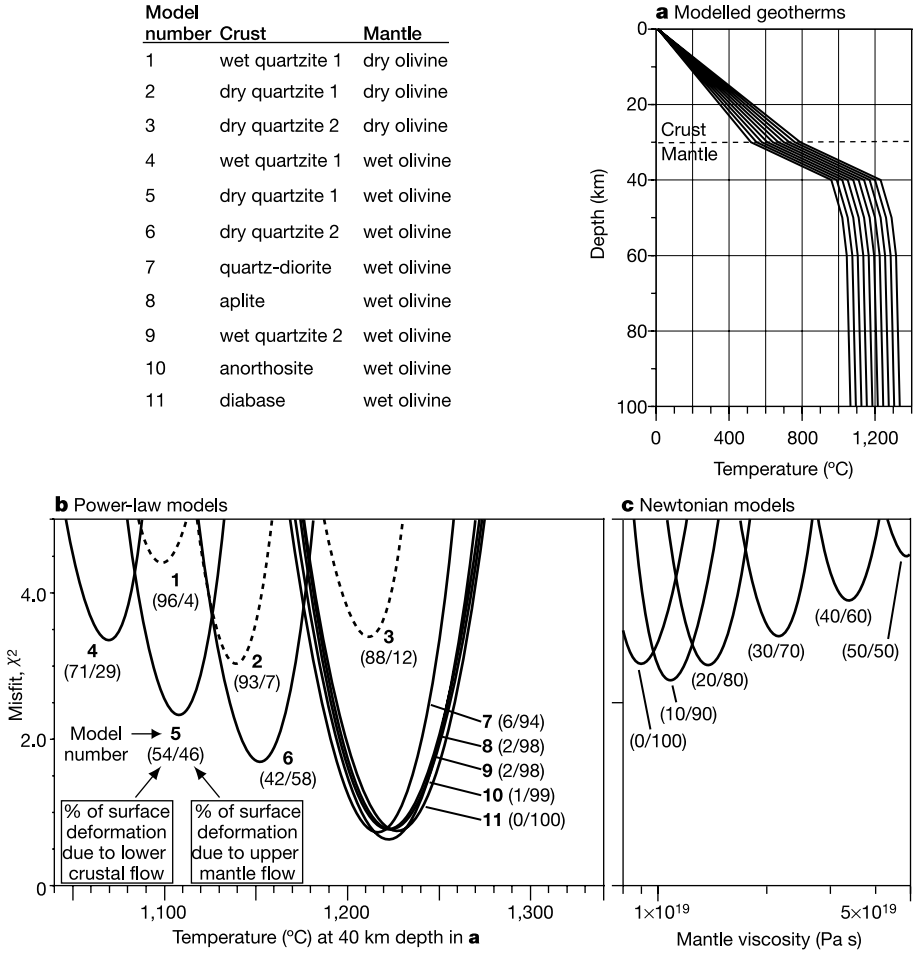

Figure 2 Testing of candidate rheologic models. Modelled geotherms (**a**) and misfits between post-Landers and post-Hector Mine GPS observed and calculated surface displacement time series for candidate power-law (**b**) and newtonian (**c**) models. Each curve in **b** represents a series of models with the same mineralogy but varying geotherm. Power-law models that consider a wet (weak) mantle are shown as solid lines, while power-law models that consider a dry (strong) mantle are shown as dotted lines. Shown with each curve is the model number from the list above and the relative surface deformation contributed by crustal and mantle flow, respectively. Assumed power laws for each rheology are shown in Table 1. Misfits for newtonian models are shown as a function of the upper mantle viscosity (30–50 km depth). Each curve in **c** represents a newtonian model with a different relative strength between the crust and mantle, denoted by the relative percentage of surface deformation induced by flow within each layer.

regions below a depth of ~18 km. We assume a shear strain rate of $0.1 \times 10^{-6}\,\mathrm{yr}^{-1}$ directed along a strike of N40° W (ref. 11). By applying this regional strain rate to the model for several hundred years before initiating the Landers earthquake, we create a pre-Landers absolute stress state consistent with the assumed thermal gradient and rheology at depths warm enough to participate in postseismic relaxation. Once steady-state stress levels are achieved, slip associated with the 1992 Landers earthquake is applied and the crust and upper mantle are allowed to relax for 7.3 years, at which time slip associated with the 1999 Hector Mine quake is imposed. Following this, the region is allowed to relax for an additional 4 years.

In addition to power-law rheologies, we also develop a series of newtonian ($n = 1$) models in order to assess the importance of the power-law exponent in explaining the observed postseismic surface deformation. Newtonian models consider an 18-km-thick elastic upper crust, a 12-km-thick viscoelastic lower crust, and a 20-km-thick viscoelastic uppermost mantle above a 100-km-thick asthenospheric layer. A single newtonian viscosity is assigned for each layer. Because of increasing temperatures with depth, we assume that the upper mantle layer has a viscosity three times greater than the asthenosphere below.

To compare modelled and observed deformation, we define the misfit χ^2 as

$$\chi^2 = \frac{1}{N}\sum_{i=1}^{N}\left\{\frac{1}{M}\sum_{j=1}^{M}\left[(\mathrm{observed}_{i,j} - \mathrm{calculated}_{i,j})^2/\sigma_{i,j}^2\right]\right\} \qquad (3)$$

where j are the individual time-series observations for each GPS station i, and the misfit is weighted by the estimated variance associated with each observation. We calculate misfits for the horizontal and vertical displacement time series following both earthquakes.

Figure 2b shows the misfit for various combinations of crustal and mantle power-law rheologies as a function of thermal gradient. The best models (lowest misfit) are those in which the percentage of surface deformation due to flow in the mantle (bottom number in parenthesis in Fig. 2b) is greatest. Thus, it is models that consider wet olivine in the upper mantle (solid curves in Fig. 2b) in conjunction with a much stronger crust, such as one composed of diabase, that provide the best fit to the data. A mantle temperature of ~1,300 °C at 50 km depth indicated by the best-fitting power law models is consistent with thermal models derived from seismic tomography of western North America[23] and evidence of a shallow asthenosphere inferred from Mojave desert xenoliths[24]. Dry olivine in conjunction with a strong crust can also provide a good match to the time-series data, but the required geotherm is far greater than that allowed by heat flow constraints. In agreement with previous studies[5,6], lower crustal flow models lead to poor fits because the predicted vertical motions are anticorrelated with GPS observations (see Supplementary Fig. 3) and the spatial extent of horizontal surface deformation is underpredicted. The goodness of fit of a power-law model of mantle flow (model 8 in Fig. 2b, $n = 3.5$) for cumulative postseismic displacements after the Landers (5.5 yr) and Hector Mine (3.2 yr) earthquakes is shown in Fig. 1 (black arrows).

In comparison to the best power-law models, newtonian models predict the GPS observations poorly (Fig. 2c). The superior fit of the power-law model can be attributed to the manner in which the viscosity of the power-law rheology increases with time as coseismic stresses diminish (equation (2)). Although deformation rates of both newtonian and power-law rheologies diminish with time, the rate decrease is much more rapid for a power-law rheology owing to this increase in viscosity. This is illustrated in Fig. 3, which shows how two distinct newtonian models, an order of magnitude different in viscosity, are required to fit early versus late periods of the time-series data. In contrast, a single power-law rheology (solid curve) can fit the time-series curvature (Supplementary Fig. 3 shows the complete set of observed and predicted GPS time series).

The stress dependence of power-law flow inferred by our calculations means that the viscosity of the upper mantle changes as a function of time after an earthquake. Thus, a newtonian viscosity inferred from a study of surface displacements for a given period of time following a particular loading event provides only limited insight into the rheologic properties of the region, and cannot be readily extrapolated to other loading conditions, time intervals or regions. Careful integration of laboratory results with geological, geophysical and geodetic measurements promises to reveal further details of the laws governing the deformation of the Earth. □

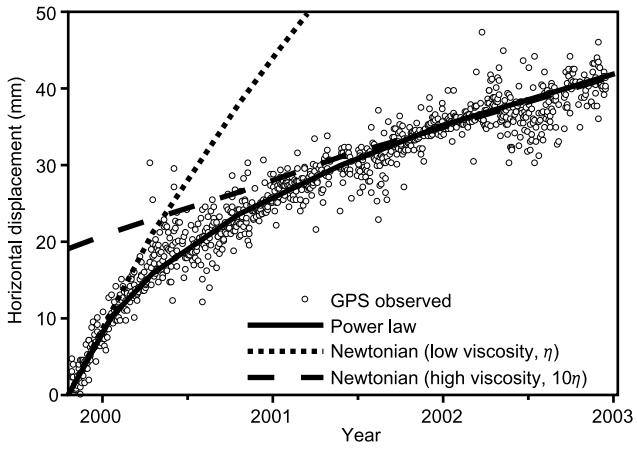

Figure 3 Comparison of representative observed and calculated postseismic displacement time series (station OPCX following the Hector Mine earthquake[12]). Power-law mantle flow model (solid curve) is model 8 in Fig. 2 (aplite, wet olivine, $T_{40\,\mathrm{km}} = 1{,}225$ °C; power-law parameters listed in Table 1). Newtonian models consider predominately mantle flow with low viscosity (2.5×10^{18} Pa s, dotted curve) and an order of magnitude higher viscosity (2.5×10^{19} Pa s, dashed curve) that match early and late time-series slopes, respectively. The curve associated with the high-viscosity newtonian model has been raised to show where the slope matches the observed time series.

Received 14 April; accepted 24 June 2004; doi:10.1038/nature02784.

1. Nur, A. & Mavko, G. Postseismic viscoelastic rebound. *Science* **183,** 204–206 (1974).
2. Kirby, S. H. & Kronenberg, A. K. Rheology of the lithosphere; selected topics. *Rev. Geophys.* **25,** 1219–1244 (1987).
3. Carter, N. L. & Tsenn, M. C. Flow properties of continental lithosphere. *Tectonophysics* **136,** 27–63 (1987).
4. Thatcher, W., Matsuda, T., Kato, T. & Rundle, J. B. Lithospheric loading by the 1896 Riku-u earthquake, northern Japan; Implications for plate flexure and asthenospheric rheology. *J. Geophys. Res.* **85,** 6429–6435 (1980).
5. Pollitz, F. F., Wicks, C. & Thatcher, W. Mantle flow beneath a continental strike-slip fault; postseismic deformation after the 1999 Hector Mine earthquake. *Science* **293,** 1814–1818 (2001).
6. Pollitz, F. F., Peltzer, G. & Bürgmann, R. Mobility of continental mantle; Evidence from postseismic geodetic observations following the 1992 Landers earthquake. *J. Geophys. Res.* **105,** 8035–8054 (2000).
7. Kenner, S. J. & Segall, P. Lower crustal structure in northern California: Implications from strain rate variations following the 1906 San Francisco earthquake. *J. Geophys. Res.* **108,** doi:101029/2001JB000189 (2003).
8. Freed, A. M. & Lin, J. Delayed triggering of the 1999 Hector Mine earthquake by viscoelastic stress transfer. *Nature* **411,** 180–183 (2001).
9. Freed, A. M. & Lin, J. Accelerated stress buildup on the southern San Andreas Fault and surrounding regions caused by Mojave Desert earthquakes. *Geology* **30,** 571–574 (2002).
10. Deng, J., Gurnis, M., Kanamori, H. & Hauksson, E. Viscoelastic flow in the lower crust after the 1992 Landers. *Science* **282,** 1689–1692 (1998).
11. Savage, J. C., Svarc, J. L. & Prescott, W. H. Near-field postseismic deformation associated with the 1992 Landers and 1999 Hector Mine, California, earthquakes. *J. Geophys. Res.* **108,** doi:101029/2002JB002330 (2003).
12. Hudnut, K. W. *et al.* Continuous GPS observations of postseismic deformation following the 16 October 1999 Hector Mine, California, earthquake. *Bull. Seismol. Soc. Am.* **92,** 1403–1422 (2002).
13. Karato, S., Paterson, M. S. & Fitzgerald, J. D. Rheology of synthetic olivine aggregates; influence of grain size and water. *J. Geophys. Res.* **91,** 8151–8176 (1986).
14. Silver, P., Mainprice, D., Ismail, W. B. & Tommasi, A. *Mantle Petrology: Field Observations and High Pressure Experimentation: A Tribute to Francis R. (Joe) Boyd* 79–103 (Geochemical Society, Spec. Publ. No. 6, Houston, Texas, 1999).
15. Hirth, G., Teyssier, C. & Dunlap, W. J. An evaluation of quartzite flow laws based on comparisons between experimentally and naturally deformed rocks. *Int. J. Earth Sci.* **90,** 77–87 (2001).

16. Pollitz, F. F. Transient rheology of the uppermost mantle beneath the Mojave Desert, California. *Earth Planet. Sci. Lett.* **215,** 89–104 (2003).
17. Wald, D. J. & Heaton, T. H. Spatial and temporal distribution of slip for the 1992 Landers, California, earthquake. *Bull. Seismol. Soc. Am.* **84,** 668–691 (1994).
18. Kaverina, A., Dreger, D. & Price, E. The combined inversion of seismic and geodetic data for the source process of the 16 October 1999 Mw 7.1 Hector Mine, California, earthquake. *Bull. Seismol. Soc. Am.* **92,** 1266–1280 (2002).
19. Masterlark, T. & Wang, H. F. Transient stress-coupling between the 1992 Landers and 1999 Hector Mine, California, earthquakes. *Bull. Seismol. Am.* **92,** 1470–1486 (2002).
20. Peltzer, G., Rosen, P. & Rogez, F. Poroelastic rebound along the Landers 1992 earthquake surface rupture. *J. Geophys. Res.* **103,** 30131–30145 (1998).
21. Williams, C. F. Temperature and the seismic/aseismic transition; observations from the 1992 Landers earthquake. *Geophys. Res. Lett.* **23,** 2029–2032 (1996).
22. Melbourne, T. & Helmberger, D. Mantle control of plate boundary deformation. *Geophys. Res. Lett.* **28,** 4003–4006 (2001).
23. Goes, S. & van der Lee, S. Thermal structure of the North American uppermost mantle inferred from seismic tomography. *J. Geophys. Res.* **107,** doi:2000JB000049 (2002).
24. Farmer, G. L. *et al.* Origin of late Cenozoic basalts at the Cima volcanic field, Mojave Desert, California. *J. Geophys. Res.* **100,** 8399–8415 (1995).
25. Kronenberg, A. K. & Tullis, J. A. Flow strengths of quartz aggregates; grain size and pressure effects due to hydrolytic weakening. *J. Geophys. Res.* **89,** 4281–4297 (1984).
26. Shelton, G. & Tullis, J. A. Experimental flow laws for crustal rocks. *Trans. Am. Geophys. Union* **62,** 396 (1981).
27. Jaoul, O., Tullis, J. A. & Kronenberg, A. K. The effect of varying water contents on the creep behaviour of Heavitree Quartzite. *J. Geophys. Res.* **89,** 4298–4312 (1984).
28. Hansen, F. D. & Carter, N. L. Creep of selected crustal rocks at 1000 MPa. *Trans. Am. Geophys. Union* **63,** 437 (1982).
29. Hirth, G. & Kohlstedt, D. Rheology of the upper mantle and the mantle wedge: A view from the experimentalists. In *The Subduction Factory* (ed. Eiler, J.) (American Geophysical Union 2004).

Supplementary Information accompanies the paper on **www.nature.com/nature**.

Acknowledgements Funding was provided by the National Science Foundation and the Southern California Earthquake Center. GPS data were provided by the US Geological Survey and the Southern California Integrated GPS Network..

Competing interests statement The authors declare that they have no competing financial interests.

Correspondence and requests for materials should be addressed to A.M.F. (freed@purdue.edu).

Fine-scale phylogenetic architecture of a complex bacterial community

Silvia G. Acinas[1]*, Vanja Klepac-Ceraj[1]*, Dana E. Hunt[1], Chanathip Pharino[1], Ivica Ceraj[2], Daniel L. Distel[3] & Martin F. Polz[1]

[1]*Department of Civil and Environmental Engineering, Massachusetts Institute of Technology, Cambridge, Massachusetts 02139, USA*
[2]*Bugaco, Somerville, Massachusetts 02144, USA*
[3]*Department of Biochemistry, Microbiology and Molecular Biology, University of Maine, Orono, Maine 04469, USA*

* These authors contributed equally to this work

Although molecular data have revealed the vast scope of microbial diversity[1], two fundamental questions remain unanswered even for well-defined natural microbial communities: how many bacterial types co-exist, and are such types naturally organized into phylogenetically discrete units of potential ecological significance? It has been argued that without such information, the environmental function, population biology and biogeography of microorganisms cannot be rigorously explored[2]. Here we address these questions by comprehensive sampling of two large 16S ribosomal RNA clone libraries from a coastal bacterioplankton community. We show that compensation for artefacts generated by common library construction techniques reveals fine-scale patterns of community composition. At least 516 ribotypes (unique rRNA sequences) were detected in the sample and, by statistical extrapolation, at least 1,633 co-existing ribotypes in the sampled population. More than 50% of the ribotypes fall into discrete clusters containing less than 1% sequence divergence. This pattern cannot be accounted for by interoperon variation, indicating a large predominance of closely related taxa in this community. We propose that such microdiverse clusters arise by selective sweeps and persist because competitive mechanisms are too weak to purge diversity from within them.

Traditional species concepts have largely been concessions to the need to identify bacteria reproducibly, but none adequately describe natural units of microbial diversity[3]. It has recently been proposed that natural taxa are distinct groups of strains that arise by periodic selection—a process of continuing, selectionally neutral, diversification punctuated by adaptive mutations leading to selective sweeps[4]. The latter events purge all sequence variants except those associated with the genome carrying the adaptive mutation[4]. One of the attractive features of this concept is that it should be applicable to molecular surveys of microbial diversity because taxa would be identifiable in phylogenetic trees as distinct clusters of closely related sequences[1]. Moreover, such clusters should be detectable independently of the gene used to construct these trees as long as the accumulation of variation is commensurate with the occurrence of sweeps[5]. However, this theory has not been applied to broad-scale studies of bacterial diversity in the environment. Over the past 20 years, diversity studies have primarily been based on analyses of 16S rRNA clone libraries but it has remained uncertain to what extent fine-scale patterns of variation are due to sequence artefacts, to heterogeneity among paralogous operons or to the co-existence of similar but differentiated taxa[1]. Furthermore, it has not been explored whether naturally defined units of differentiation emerge from recently released shotgun sequence data from the Sargasso Sea[6].

We deduced that the discovery of ecologically significant patterns of relationships between co-existing ribotypes requires, first, an examination of clone libraries large enough to elucidate relationships at all levels of differentiation, and second, methods that minimize and account for the contribution of sequence artefacts and paralogous variation to diversity estimates. We sequenced about 1,000 clones from each of two polymerase chain reaction (PCR)-derived 16S rRNA libraries constructed from the same coastal bacterioplankton sample. The first library employed common (standard) amplification protocols. For the second, a modified protocol was designed to minimize artefacts and to identify Taq errors and chimaeric molecules through extensive sequence analyses (see Methods). This approach allowed the most comprehensive analysis of any single gene from co-occurring populations so far, even in view of the recently released Sargasso Sea study, which in aggregate sampled a similar number of rRNA genes but from several locations, dates and diverse biogeochemical conditions[6]. Our overall rationale was to achieve high coverage of rRNA genes from a single community while estimating and compensating for the influence of artefacts on ribotype diversity, potentially revealing emergent patterns.

Comparison of the two libraries showed that changes to the amplification protocol alone decreased the incidence of unique sequences from 76% (692 of 909) in the standard to 61% (686 of 1,131) in the modified library. Correction for chimaeras and Taq error lowered the percentage to 48% (516 of 1,067) unique sequences (Fig. 1a), demonstrating a potentially significant contribution of PCR-induced artefacts to (micro)diversity estimates. Consequently, these corrections yield a significantly lower estimate of total ribotype diversity for the sampled community when compared with the unmodified standard library (1,633 versus 3,881) with the use of the Chao-1 estimator[7]. A novel estimator (N_T/N_{max}) (ref. 2) yielded a similar value of 2,236 sequences for the corrected data set. This good agreement, combined with the low incidence of chimaeras and the observation that corrections account